

# Study of the heavy CP-even Higgs with mass 125 GeV in two-Higgs-doublet models at the LHC and ILC

Lei Wang, Xiao-Fang Han

*Department of Physics, Yantai University, Yantai 264005, PR China*

## Abstract

We assume that the 125 GeV Higgs discovered at the LHC is the heavy CP-even Higgs of the two-Higgs-doublet models, and examine the parameter space in the Type-I, Type-II, Lepton-specific and Flipped models allowed by the latest Higgs signal data, the relevant experimental and theoretical constraints. Further, we show the projected limits on  $\tan\beta$ ,  $\sin(\beta - \alpha)$ ,  $Hf\bar{f}$  and  $HVV$  couplings from the future measurements of the 125 GeV Higgs at the LHC and ILC, including the LHC with integrated luminosity of  $300 \text{ fb}^{-1}$  (LHC-300  $\text{fb}^{-1}$ ) and  $3000 \text{ fb}^{-1}$  (LHC-3000  $\text{fb}^{-1}$ ) as well as the ILC at  $\sqrt{s} = 250 \text{ GeV}$  (ILC-250 GeV),  $\sqrt{s} = 500 \text{ GeV}$  (ILC-500 GeV) and  $\sqrt{s} = 1000 \text{ GeV}$  (ILC-1000 GeV). Assuming that the future Higgs signal data have no deviation from the SM expectation, the LHC-300  $\text{fb}^{-1}$ , LHC-3000  $\text{fb}^{-1}$  and ILC-1000 GeV can exclude the wrong-sign Yukawa coupling regions of the Type-II, Flipped and Lepton-specific models at the  $2\sigma$  level, respectively. The future experiments at the LHC and ILC will constrain the Higgs couplings to be very close to SM values, especially for the  $HVV$  coupling.

PACS numbers: 12.60.Fr, 14.80.Ec, 14.80.Bn

## I. INTRODUCTION

A 125 GeV Higgs boson has been discovered in the ATLAS and CMS experiments at the LHC [1, 2]. A number of new measurements or updates of existing ones were presented in ICHEP 2014 [3, 4]. Especially the diphoton signal strength is changed from  $1.6 \pm 0.4$  to  $1.17 \pm 0.27$  for ATLAS [5] and from  $0.78_{-0.16}^{+0.28}$  to  $1.12_{-0.32}^{+0.37}$  for CMS [6]. There are some updates in the  $ZZ$  [7, 8],  $WW$  [9, 10],  $b\bar{b}$  [11],  $\tau\bar{\tau}$  [12] decay modes, and the  $t\bar{t}H$  events [13, 14] from ATLAS and CMS, as well as an overall update from the D0 [15] since 2013. The properties of this particle with large experimental uncertainties agree with the Standard Model (SM) predictions. The two-Higgs-doublet model (2HDM) has very rich Higgs phenomenology, including two neutral CP-even Higgs bosons  $h$  and  $H$ , one neutral pseudoscalar  $A$ , and two charged Higgs  $H^\pm$ . There are four traditional types for 2HDMs, Type-I [16, 17], Type-II [16, 18], Lepton-specific, and Flipped models [19–24] according to their different Yukawa couplings, in which the tree-level flavor changing neutral currents (FCNC) are forbidden by a discrete symmetry. In addition, there is no tree-level FCNC in the 2HDM that allows both doublets to couple to the fermions with aligned Yukawa matrices [25]. The recent Higgs data have been used to constrain these 2HDMs over the last few months [26–55].

In this paper, we assume that the 125 GeV Higgs discovered at the LHC is respectively the heavy CP-even Higgs of the Type-I, Type-II, Lepton-specific and Flipped 2HDMs, and examine the parameter space allowed by the latest Higgs signal data, the non-observation of additional Higgs at the collider, and the theoretical constraints from vacuum stability, unitarity and perturbativity as well as the experimental constraints from the electroweak precision data and flavor observables. Further, we analyze how well 2HDMs can be distinguished from SM by the future measurements of the 125 GeV Higgs at the LHC and ILC, including the LHC with the center of mass energy  $\sqrt{s} = 14$  TeV and integrated luminosity of  $300 \text{ fb}^{-1}$  (LHC-300  $\text{fb}^{-1}$ ) and  $3000 \text{ fb}^{-1}$  (LHC-3000  $\text{fb}^{-1}$ ) as well as the ILC at  $\sqrt{s} = 250$  GeV (ILC-250 GeV),  $\sqrt{s} = 500$  GeV (ILC-500 GeV) and  $\sqrt{s} = 1000$  GeV (ILC-1000 GeV). For the 125 GeV Higgs is the light CP-even Higgs, the projected limits on 2HDMs from the future measurements of the 125 GeV Higgs at the LHC and ILC have been studied in [40, 41].

Our work is organized as follows. In Sec. II we recapitulate the two-Higgs-doublet models. In Sec. III we introduce the numerical calculations. In Sec. IV, we examine the implications

of the latest Higgs signal data on the 2HDMs and projected limits on the 2HDMs from the future measurements of the 125 GeV Higgs at the LHC and ILC after imposing the theoretical and experimental constraints. Finally, we give our conclusion in Sec. V.

## II. TWO-HIGGS-DOUBLET MODELS

The Higgs potential with a softly broken  $Z_2$  symmetry is written as [56]

$$\begin{aligned} V = & m_{11}^2(\Phi_1^\dagger\Phi_1) + m_{22}^2(\Phi_2^\dagger\Phi_2) - \left[ m_{12}^2(\Phi_1^\dagger\Phi_2 + \text{h.c.}) \right] \\ & + \frac{\lambda_1}{2}(\Phi_1^\dagger\Phi_1)^2 + \frac{\lambda_2}{2}(\Phi_2^\dagger\Phi_2)^2 + \lambda_3(\Phi_1^\dagger\Phi_1)(\Phi_2^\dagger\Phi_2) + \lambda_4(\Phi_1^\dagger\Phi_2)(\Phi_2^\dagger\Phi_1) \\ & + \left[ \frac{\lambda_5}{2}(\Phi_1^\dagger\Phi_2)^2 + \text{h.c.} \right]. \end{aligned} \quad (1)$$

We focus on the CP-conserving model in which all  $\lambda_i$  and  $m_{12}^2$  are real. The two complex scalar doublets have the hypercharge  $Y = 1$ ,

$$\Phi_1 = \begin{pmatrix} \phi_1^+ \\ \frac{1}{\sqrt{2}}(v_1 + \phi_1^0 + ia_1) \end{pmatrix}, \quad \Phi_2 = \begin{pmatrix} \phi_2^+ \\ \frac{1}{\sqrt{2}}(v_2 + \phi_2^0 + ia_2) \end{pmatrix}. \quad (2)$$

Where the electroweak vacuum expectation values (VEVs)  $v^2 = v_1^2 + v_2^2 = (246 \text{ GeV})^2$ , and the ratio of the two VEVs is defined as usual to be  $\tan\beta = v_2/v_1$ . After spontaneous electroweak symmetry breaking, there are five mass eigenstates: two neutral CP-even  $h$  and  $H$ , one neutral pseudoscalar  $A$ , and two charged scalar  $H^\pm$ .

The tree-level couplings of the neutral Higgs bosons can have sizable deviations from those of SM Higgs boson. Table I shows the couplings of the heavy CP-even Higgs with respect to those of the SM Higgs boson in the Type-I, Type-II, Lepton-specific and Flipped models.

## III. NUMERICAL CALCULATIONS

Using the method taken in [57–64], we perform a global fit to the latest Higgs data of 29 channels (see Tables I-V in [65]). The signal strength for the  $i$  channel is defined as

$$\mu_i = \epsilon_{ggh}^i R_{ggh} + \epsilon_{VBF}^i R_{VBF} + \epsilon_{VH}^i R_{VH} + \epsilon_{t\bar{t}H}^i R_{t\bar{t}H}. \quad (3)$$

TABLE I: The tree-level couplings of the heavy CP-even Higgs with respect to those of the SM Higgs boson.  $u$ ,  $d$  and  $l$  denote the up-type quarks, down-type quarks and the charged leptons, respectively.

model	$HVV$ ( $WW$ , $ZZ$ )	$Hu\bar{u}$	$Hd\bar{d}$	$Hl\bar{l}$
Type-I	$\cos(\beta - \alpha)$	$\frac{\sin \alpha}{\sin \beta}$	$\frac{\sin \alpha}{\sin \beta}$	$\frac{\sin \alpha}{\sin \beta}$
Type-II	$\cos(\beta - \alpha)$	$\frac{\sin \alpha}{\sin \beta}$	$\frac{\cos \alpha}{\cos \beta}$	$\frac{\cos \alpha}{\cos \beta}$
Lepton-specific	$\cos(\beta - \alpha)$	$\frac{\sin \alpha}{\sin \beta}$	$\frac{\sin \alpha}{\sin \beta}$	$\frac{\cos \alpha}{\cos \beta}$
Flipped	$\cos(\beta - \alpha)$	$\frac{\sin \alpha}{\sin \beta}$	$\frac{\cos \alpha}{\cos \beta}$	$\frac{\sin \alpha}{\sin \beta}$

Where  $R_j = \frac{(\sigma \times BR)_j}{(\sigma \times BR)_j^{SM}}$  with  $j$  denoting the partonic processes  $ggH$ ,  $VBF$ ,  $VH$ , and  $t\bar{t}H$ .  $\epsilon_j^i$  denotes the assumed signal composition of the partonic process  $j$ , which are given in Tables I-V of [65]. The  $\chi^2$  for an uncorrelated observable is

$$\chi_i^2 = \frac{(\mu_i - \mu_i^{exp})^2}{\sigma_i^2}, \quad (4)$$

where  $\mu_i^{exp}$  and  $\sigma_i$  denote the experimental central value and uncertainty for the  $i$  channel. The uncertainty asymmetry is retained in our calculations. For the two correlated observables, we use

$$\chi_{i,j}^2 = \frac{1}{1 - \rho^2} \left[ \frac{(\mu_i - \mu_i^{exp})^2}{\sigma_i^2} + \frac{(\mu_j - \mu_j^{exp})^2}{\sigma_j^2} - 2\rho \frac{(\mu_i - \mu_i^{exp})}{\sigma_i} \frac{(\mu_j - \mu_j^{exp})}{\sigma_j} \right], \quad (5)$$

where  $\rho$  is the correlation coefficient. We sum over the  $\chi^2$  for the 29 channels, and pay particular attention to the surviving samples with  $\chi^2 - \chi_{\min}^2 \leq 6.18$ , where  $\chi_{\min}^2$  denotes the minimum of  $\chi^2$ . These samples correspond to the 95.4% confidence level regions in any two dimensional plane of the model parameters when explaining the Higgs data (corresponding to be within  $2\sigma$  range).

We employ 2HDMC-1.6.4 [66] to implement the theoretical constraints from the vacuum stability, unitarity and coupling-constant perturbativity, and calculate the oblique parameters ( $S$ ,  $T$ ,  $U$ ) and  $\delta\rho$ , whose experimental data are from Ref. [67].  $\delta\rho$  has been precisely measured to be very close to 1 via Z-pole precision observables, which gives a strong constraint on the mass difference between various Higgses in the 2HDMs. SuperIso-3.3 [68] is used to implement the constraints from flavor observables, including  $B \rightarrow X_s \gamma$  [69],  $B_s \rightarrow \mu^+ \mu^-$  [70],  $B_u \rightarrow \tau \nu$  [71] and  $D_s \rightarrow \tau \nu$  [69]. HiggsBounds-4.1.3 [72, 73] is employed to



TABLE II: Projected  $1\sigma$  sensitivities of channels for the LHC operating  $\sqrt{s} = 14$  TeV. The  $300 \text{ fb}^{-1}$  and  $3000 \text{ fb}^{-1}$  sensitivities are taken from Ref. [81] for ATLAS and Ref. [82] for CMS. The assumed signal composition is taken from Ref. [80].

Channel	Projected $1\sigma$ sensitivity		Assumed signal composition (%)				
	$300 \text{ fb}^{-1}$	$3000 \text{ fb}^{-1}$	ggH	VBF	WH	ZH	$t\bar{t}H$
ATL ( $pp$ ) $\rightarrow h \rightarrow \gamma\gamma$ (0jet)	0.22	0.20	91.6	2.7	3.2	1.8	0.6
ATL ( $pp$ ) $\rightarrow h \rightarrow \gamma\gamma$ (1jet)	0.37	0.37	81.8	13.2	2.9	1.6	0.5
ATL ( $pp$ ) $\rightarrow h \rightarrow \gamma\gamma$ (VBF-like)	0.47	0.21	39.2	58.4	1.4	0.8	0.3
ATL ( $pp$ ) $\rightarrow h \rightarrow \gamma\gamma$ ( $VH$ -like)	0.77	0.26	2.5	0.4	63.3	15.2	18.7
ATL ( $pp$ ) $\rightarrow h \rightarrow \gamma\gamma$ ( $t\bar{t}H$ -like)	0.55	0.21	0.0	0.0	0.0	0.0	100.0
ATL ( $pp$ ) $\rightarrow h \rightarrow WW$ (0jet)	0.20	0.19	98.2	1.8	0.0	0.0	0.0
ATL ( $pp$ ) $\rightarrow h \rightarrow WW$ (1jet)	0.36	0.33	88.4	11.6	0.0	0.0	0.0
ATL ( $pp$ ) $\rightarrow h \rightarrow WW$ (VBF-like)	0.21	0.12	8.1	91.9	0.0	0.0	0.0
ATL ( $pp$ ) $\rightarrow h \rightarrow ZZ$ (ggF-like)	0.13	0.12	88.7	7.2	2.0	1.4	0.7
ATL ( $pp$ ) $\rightarrow h \rightarrow ZZ$ (VBF-like)	0.34	0.21	44.7	53.2	0.7	0.4	1.0
ATL ( $pp$ ) $\rightarrow h \rightarrow ZZ$ ( $VH$ -like)	0.32	0.13	30.1	9.0	34.8	12.1	14.0
ATL ( $pp$ ) $\rightarrow h \rightarrow ZZ$ ( $t\bar{t}H$ -like)	0.46	0.20	8.7	1.7	1.7	3.1	84.8
ATL ( $pp$ ) $\rightarrow h \rightarrow Z\gamma$	1.47	0.57	87.6	7.1	3.1	1.7	0.6
ATL ( $pp$ ) $\rightarrow h \rightarrow \mu\mu$	0.47	0.19	87.6	7.1	3.1	1.7	0.6
ATL ( $pp$ ) $\rightarrow h \rightarrow \mu\mu$ ( $t\bar{t}H$ )	0.73	0.26	0.0	0.0	0.0	0.0	100.0
ATL ( $pp$ ) $\rightarrow h \rightarrow \tau\tau$ (VBF-like)	0.22	0.19	19.8	80.2	0.0	0.0	0.0
CMS ( $pp$ ) $\rightarrow h \rightarrow \gamma\gamma$	0.06	0.04	87.6	7.1	3.1	1.7	0.6
CMS ( $pp$ ) $\rightarrow h \rightarrow WW$	0.06	0.04	88.1	7.1	3.1	1.7	0.0
CMS ( $pp$ ) $\rightarrow h \rightarrow ZZ$	0.07	0.04	88.1	7.1	3.1	1.7	0.0
CMS ( $pp$ ) $\rightarrow h \rightarrow Z\gamma$	0.62	0.20	87.6	7.1	3.1	1.7	0.6
CMS ( $pp$ ) $\rightarrow h \rightarrow b\bar{b}$	0.11	0.05	0.0	0.0	57.0	32.3	10.7
CMS ( $pp$ ) $\rightarrow h \rightarrow \mu\mu$	0.40	0.20	87.6	7.1	3.1	1.7	0.6
CMS ( $pp$ ) $\rightarrow h \rightarrow \tau\tau$	0.08	0.05	68.6	27.7	2.4	1.4	0.0

implement the exclusion constraints from the neutral and charged Higgses searches at LEP, Tevatron and LHC at 95% confidence level. The constraints from  $\Delta m_{B_d}$  and  $\Delta m_{B_s}$  [74] are considered, which are calculated using the formulas in [75]. In addition,  $R_b$  is calculated by

$$R_b \equiv (1 + \frac{S_b^{SM}}{s_b^{SM} + \delta s_b} C_b)^{-1} = R_b^{SM} (1 + \frac{\delta s_b}{s_b^{SM}}) / (1 + R_b^{SM} \frac{\delta s_b}{s_b^{SM}}), \quad (6)$$

where

$$s_b^{SM} = [(\bar{g}_b^L - \bar{g}_b^R)^2 + (\bar{g}_b^L + \bar{g}_b^R)^2] (1 + \frac{3\alpha}{4\pi} Q_b^2), \quad \delta s_b = s_b - s_b^{SM}. \quad (7)$$

We take the SM value  $R_b^{SM} = 0.21550 \pm 0.00003$  [76] and the experimental data  $R_b^{exp} = 0.21629 \pm 0.00066$  [77]. Following the calculations of Ref. [78], we can obtain the contributions of the charged and neutral Higgses to the tree-level couplings  $\bar{g}_b^L$  and  $\bar{g}_b^R$ , and the QCD corrections is included, whose expressions are given in Ref. [79].

The measurement uncertainties of Higgs signal rates will be sizably reduced at the LHC-300 fb<sup>-1</sup> and LHC-3000 fb<sup>-1</sup>. The projected 1 $\sigma$  sensitivities for channels are shown in Table II. The sensitivities of ATLAS include the current theory systematic uncertainties, the statistical and experimental systematic uncertainties. The sensitivities of ATLAS taken in Ref. [80] does not include the theory uncertainty. Therefore, the sensitivities of ATLAS in Table II differ considerably from those in Ref. [80]. The sensitivities of CMS correspond to Scenario 2, which extrapolates the analyses of 7 and 8 TeV data to 14 TeV assuming the theory uncertainties will be reduced by a factor of 2 while other uncertainties are reduced by a factor of  $1/\sqrt{\mathcal{L}}$ . The assumed signal composition is taken from Ref. [80], which obtains the signal composition for ATLAS from Refs. [81, 83], and assumes typical values of the signal composition for CMS guided by present LHC measurements since CMS does not provide the signal composition.

Using the projected 1 $\sigma$  sensitivities for channels, we define

$$\chi^2 = \sum_i \frac{(\epsilon_{ggh}^i R_{ggh} + \epsilon_{VBF}^i R_{VBF} + \epsilon_{WH}^i R_{WH} + \epsilon_{ZH}^i R_{ZH} + \epsilon_{t\bar{t}H}^i R_{t\bar{t}H} - 1)^2}{\sigma_i^2}. \quad (8)$$

Where  $R_j = \frac{(\sigma \times BR)_j}{(\sigma \times BR)_j^{SM}}$  with  $j$  denoting the partonic processes  $ggh$ ,  $VBF$ ,  $WH$ ,  $ZH$  and  $t\bar{t}H$ .  $\epsilon_j^i$  and  $\sigma_i$  denote the assumed signal composition of the partonic process  $j$  and 1 $\sigma$  uncertainty for the signal  $i$ , respectively. Thus,  $\chi^2$  is used to determine how well 2HDMs can be distinguished from the SM by the future measurement of the 125 GeV Higgs at the LHC. In another words, we assume the future Higgs signal data have no deviation from the

TABLE III: Projected  $1\sigma$  sensitivities of channels for the ILC operating at  $\sqrt{s} = 250$  GeV, 500 GeV and 1000 GeV with a corresponding integrated luminosity of  $250 \text{ fb}^{-1}$ ,  $500 \text{ fb}^{-1}$  and  $1000 \text{ fb}^{-1}$ , respectively [84].

Channel	250 GeV	500 GeV	1 TeV
$\mu_{Zh}$	2.6%	3.0%	–
$\mu_{Zh}(b\bar{b})$	1.2%	1.8%	–
$\mu_{Zh}(c\bar{c})$	8.3%	13%	–
$\mu_{Zh}(gg)$	7.0%	11%	–
$\mu_{Zh}(WW)$	6.4%	9.2%	–
$\mu_{Zh}(ZZ)$	18%	25%	–
$\mu_{Zh}(\tau\tau)$	4.2%	5.4%	–
$\mu_{Zh}(\gamma\gamma)$	34%	34%	–
$\mu_{Zh}(\mu\mu)$	100%	–	–
$\mu_{WW}(b\bar{b})$	10.5%	0.7%	0.5%
$\mu_{WW}(c\bar{c})$	–	6.2%	3.1%
$\mu_{WW}(gg)$	–	4.1%	2.6%
$\mu_{WW}(WW)$	–	2.4%	1.6%
$\mu_{WW}(ZZ)$	–	8.2%	4.1%
$\mu_{WW}(\tau\tau)$	–	9.0%	3.1%
$\mu_{WW}(\gamma\gamma)$	–	23%	8.5%
$\mu_{WW}(\mu\mu)$	–	–	31%
$\mu_{t\bar{t}}(b\bar{b})$	–	28%	6.0%

SM expectation, and estimate the limits on the 2HDMs using the projected  $1\sigma$  uncertainties for channels at the LHC-300  $\text{fb}^{-1}$  and LHC-3000  $\text{fb}^{-1}$ .

On the other hand, the design center of mass energy at the International Linear Collider (ILC) are 250 GeV and 500 GeV with a possibility to upgrade to 1 TeV. For the Higgs measurements, the beam polarizations are tuned to be  $(e^-, e^+) = (-0.8, +0.3)$  at 250 GeV and 500 GeV as well as  $(e^-, e^+) = (-0.8, +0.2)$  at 1 TeV. At  $\sqrt{s} = 250$  GeV, an absolute measurement of the production cross section can be performed from the  $Z$  Higgsstrahlung

near threshold. The weak boson fusion process dominates over the  $Z$  Higgsstrahlung process at 500 GeV and 1000 GeV. The projected  $1\sigma$  sensitivities of channels at the ILC are shown in Table III. Using the projected  $1\sigma$  sensitivities for channels at the ILC, we define

$$\chi^2 = \sum_i \frac{(R_i - 1)^2}{\sigma_i^2}, \quad (9)$$

where  $R_i$  and  $\sigma_i$  represent the signal strength prediction from the 2HDMs and the  $1\sigma$  uncertainty for the signal  $i$ , respectively.

In our calculations, the input parameters are taken as  $m_{12}^2$ ,  $\tan\beta$ ,  $\sin(\beta - \alpha)$  and the physical Higgs masses ( $m_h$ ,  $m_H$ ,  $m_A$ ,  $m_{H^\pm}$ ). We fix  $m_H$  as 125 GeV, and scan randomly the parameters in the following ranges:

$$\begin{aligned} 20 \text{ GeV} &\leq m_h \leq 125 \text{ GeV}, & 50 \text{ GeV} &\leq m_A, m_{H^\pm} \leq 800 \text{ GeV}, \\ -0.7 &\leq \sin(\beta - \alpha) \leq 0.7, & 0.1 &\leq \tan\beta \leq 40, \\ -(400 \text{ GeV})^2 &\leq m_{12}^2 \leq (400 \text{ GeV})^2. \end{aligned} \quad (10)$$

#### IV. RESULTS AND DISCUSSIONS

In addition to that the theoretical constraints are satisfied, we require the 2HDMs to explain the experimental data of flavor observables and the electroweak precision data within  $2\sigma$  range, and fit the current Higgs signal data, the future LHC and ILC data at the  $2\sigma$  level.

In Fig. 1, we project the surviving samples on the plane of  $\sin(\beta - \alpha)$  versus  $\tan\beta$ .  $\tan\beta$  is required to be larger than 1.6 for the Type-I and Lepton-specific models, and 1.1 for the Type-II and Flipped models. The main constraints are from  $\Delta m_{B_d}$  and  $\Delta m_{B_s}$  which are sensitive to  $\cot\beta$ . The Type-I model is less constrained than the other three models by the current data.  $\sin(\beta - \alpha)$  is allowed to vary in the range of -0.55 and 0.5. In the Type-I model, the neutral CP-even Higgs couplings to fermions have a universal varying factor. In addition, the charged Higgs Yukawa couplings approach to zero in the large  $\tan\beta$  limit, which is less constrained by  $B \rightarrow X_s \gamma$  and  $R_b$ .

Fig. 1 shows that the surviving samples lie in the two different regions in the Type-II, Lepton-specific and Flipped models. In one region, the 125 GeV Higgs couplings are near the SM values, called SM-like region. In the other region, at least one of the Higgs Yukawa

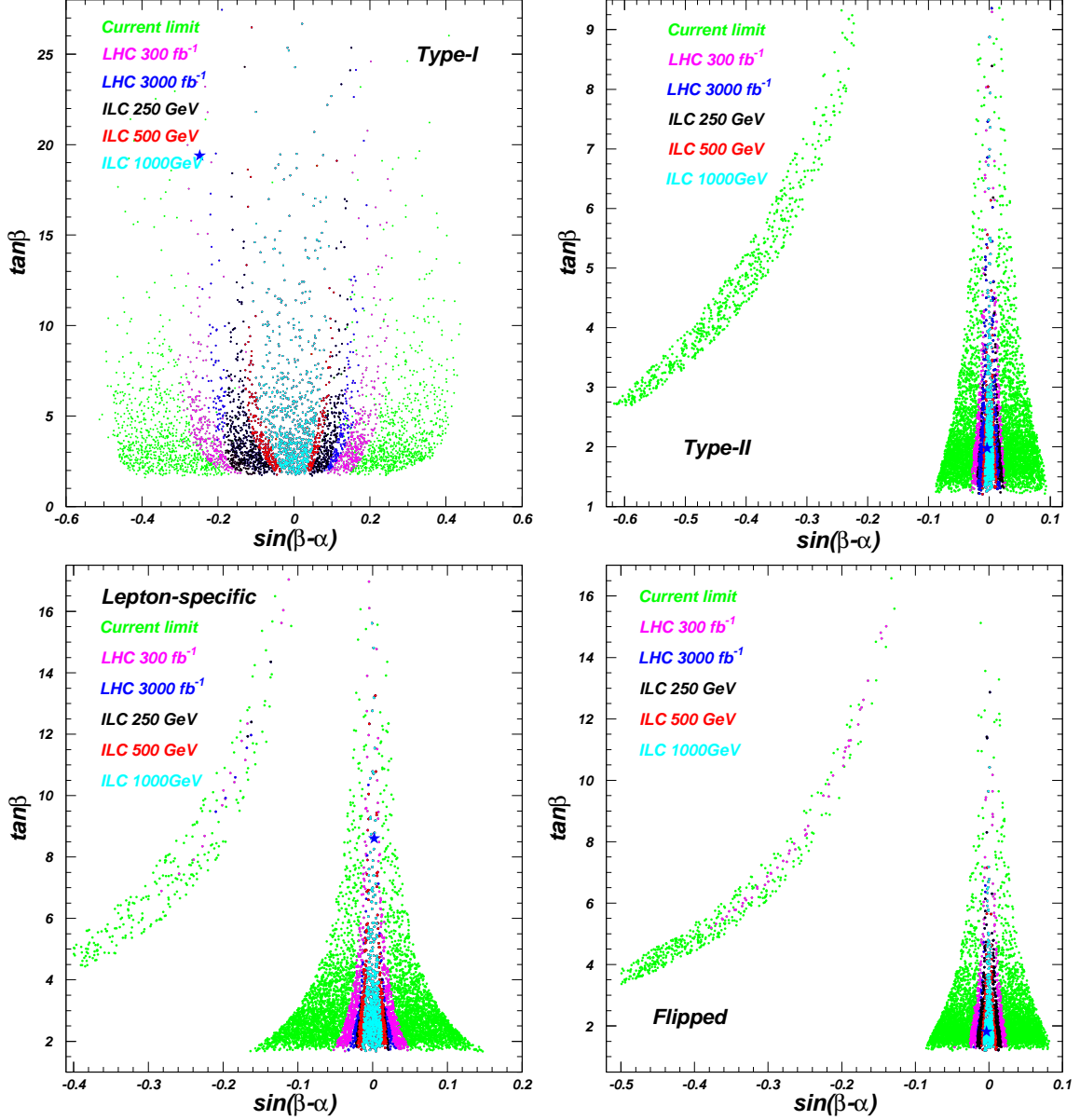


FIG. 1: The scatter plots of surviving samples projected on the planes of  $\sin(\beta - \alpha)$  versus  $\tan \beta$ . The samples with the minimal values of  $\chi^2$  are marked out as stars.

couplings has opposite sign to the corresponding coupling to VV, called wrong-sign Yukawa coupling region. Now we analyze the two regions in detail. In the four models, there are two factors of  $\frac{\cos \alpha}{\cos \beta}$  and  $\frac{\sin \alpha}{\sin \beta}$  for the heavy CP-even Higgs Yukawa couplings normalized to the corresponding SM values.

For  $\frac{\sin \alpha}{\sin \beta}$ ,

$$\frac{\sin \alpha}{\sin \beta} = \cos(\beta - \alpha) - \sin(\beta - \alpha) \cot \beta. \quad (11)$$

In the wrong-sign Yukawa coupling region where both  $|\varepsilon|$  and  $\sin^2(\beta - \alpha)$  are much smaller than 1,

$$\frac{\sin \alpha}{\sin \beta} = -1 + \varepsilon, \quad \cos(\beta - \alpha) \simeq 1 - \frac{1}{2} \sin^2(\beta - \alpha)^2. \quad (12)$$

From Eqs. (11) and (12), we obtain

$$\tan \beta = \frac{2 \sin(\beta - \alpha)}{4 - 2\varepsilon - \sin^2(\beta - \alpha)}. \quad (13)$$

This implies the wrong-sign  $hf\bar{f}$  coupling with a normalized factor  $\frac{\sin \alpha}{\sin \beta}$  can only be achieved for  $\tan \beta$  is much smaller than 1, which is excluded by the current experimental data as the above discussions.

For  $\frac{\cos \alpha}{\cos \beta}$ ,

$$\frac{\cos \alpha}{\cos \beta} = \cos(\beta - \alpha) + \sin(\beta - \alpha) \tan \beta, \quad (14)$$

$$\frac{\cos \alpha}{\cos \beta} = \cos(\beta + \alpha) + \sin(\beta + \alpha) \tan \beta. \quad (15)$$

For  $\cos(\beta - \alpha) = 1$  and  $\cos(\beta + \alpha) = -1$ , the  $Hf\bar{f}$  couplings normalize to the SM value equal to 1 and -1, which are the limiting cases of the SM-like region and the wrong-sign Yukawa coupling region, respectively.

In the wrong-sign Yukawa coupling region where both  $|\varepsilon|$  and  $\sin^2(\beta - \alpha)$  are much smaller than 1,

$$\frac{\cos \alpha}{\cos \beta} = -1 + \varepsilon, \quad \cos(\beta - \alpha) \simeq 1 - \frac{1}{2} \sin^2(\beta - \alpha)^2. \quad (16)$$

From Eqs. (14) and (16), we obtain

$$\tan \beta = \frac{\frac{1}{2} \sin(\beta - \alpha)^2 + \varepsilon - 2}{\sin(\beta - \alpha)}, \quad (17)$$

$$\sin(\beta - \alpha) = \frac{\frac{1}{2} \sin(\beta - \alpha)^2 + \varepsilon - 2}{\tan \beta}. \quad (18)$$

From Eq. (17), the wrong-sign  $hf\bar{f}$  coupling with a normalized factor  $\frac{\cos \alpha}{\cos \beta}$  can only be achieved for  $\tan \beta$  is much larger than 1 and  $\sin(\beta - \alpha) < 0$ .

In the SM-like region,

$$\frac{\cos \alpha}{\cos \beta} = 1 - \varepsilon, \quad \cos(\beta - \alpha) \simeq 1 - \frac{1}{2} \sin^2(\beta - \alpha)^2. \quad (19)$$

From Eqs. (14) and (19), we obtain

$$\tan \beta = \frac{\frac{1}{2} \sin(\beta - \alpha)^2 - \varepsilon}{\sin(\beta - \alpha)}, \quad (20)$$

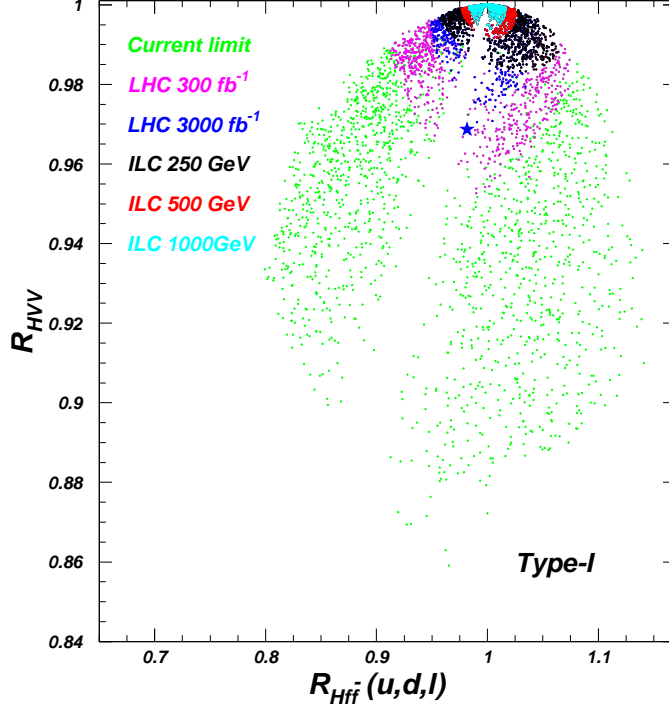


FIG. 2: The scatter plots of surviving samples in the Type-I model projected on the planes of  $R_{Hf\bar{f}}(u,d,l)$  versus  $R_{HVV}$ . Where  $R_{Hf\bar{f}}$  and  $R_{HVV}$  denote the heavy CP-even Higgs couplings to  $f\bar{f}$  and  $VV$  normalized to the corresponding SM values.

$$\sin(\beta - \alpha) = \frac{\frac{1}{2}\sin(\beta - \alpha)^2 - \varepsilon}{\tan \beta}. \quad (21)$$

Compared Eqs. (17) and (20), the lower bound of  $\tan \beta$  in the wrong-sign Yukawa coupling region should be larger than that in the SM-like region. Compared Eqs. (18) and (21), the absolute value of  $\sin(\beta - \alpha)$  in the wrong-sign Yukawa coupling region should be larger than that in the SM-like region for the same  $\tan \beta$ . Recently, Ref. [42] discusses the wrong-sign Yukawa coupling of the light CP-even Higgs in the Type-II model in detail.

Therefore, the wrong-sign Yukawa coupling can be achieved for the  $hdd\bar{d}$  and  $hll\bar{l}$  couplings in the Type-II model,  $hll\bar{l}$  in the Lepton-specific model, and  $hdd\bar{d}$  in the Flipped model. The above analyses are confirmed by what are shown in the Fig. 1. In the wrong-sign Yukawa coupling regions, the current data require  $\tan \beta > 2.5$  for the Type-II model,  $\tan \beta > 4$  for the Lepton-specific model and  $\tan \beta > 3$  for the Flipped model.  $\sin(\beta - \alpha)$  is allowed to be as low as -0.62 for the Type-II model, -0.4 for the Lepton-specific model and -0.5 for the Flipped model. In the SM-like regions, the current data require  $-0.18 < \sin(\beta - \alpha) < 0.16$  for the Lepton-specific model, and  $-0.1 < \sin(\beta - \alpha) < 0.1$  for the Type-II model and the

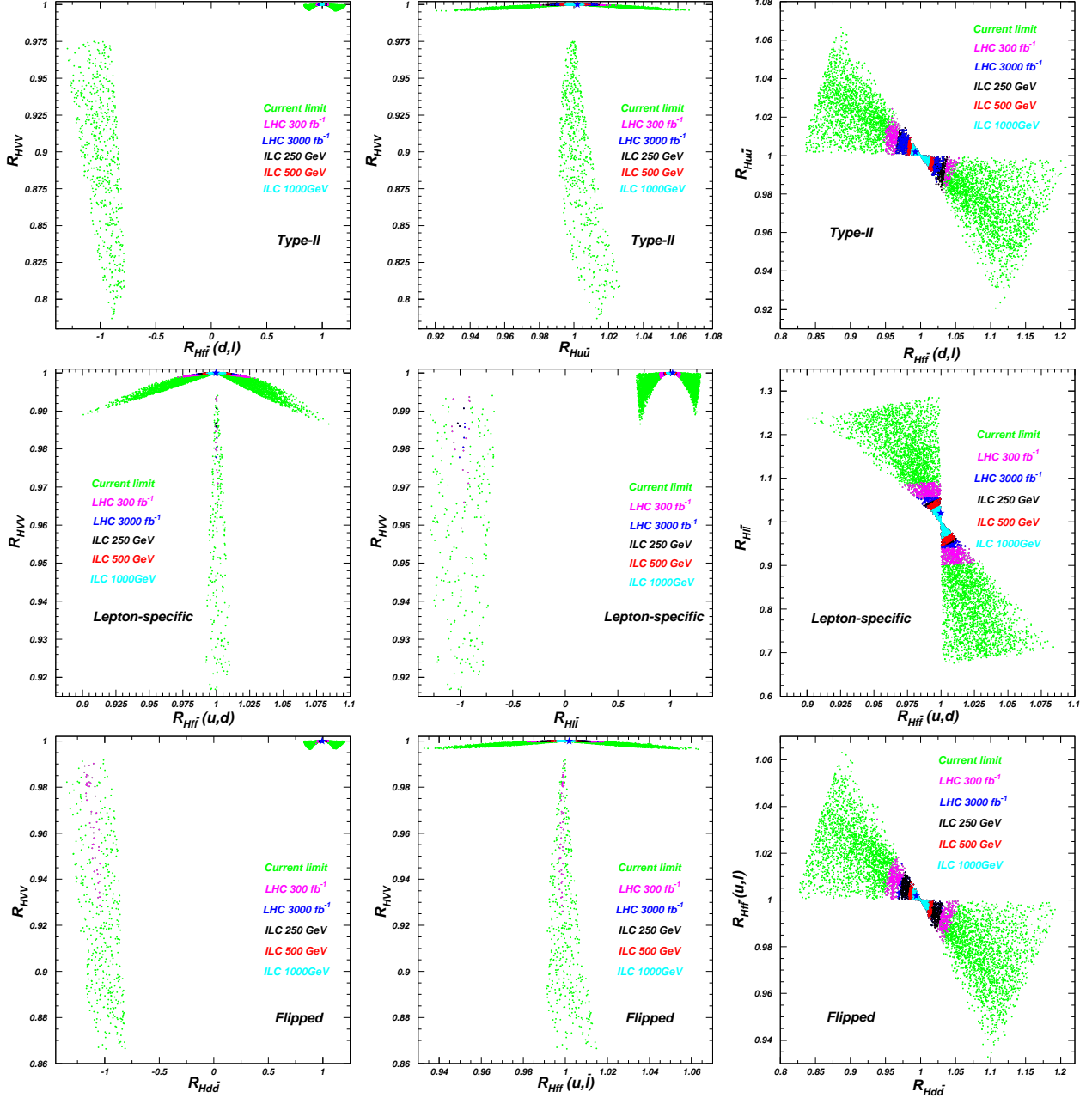


FIG. 3: Same as Fig. 2, but for the Type-II, Lepton-specific and Flipped models.

Flipped model.

For the Type-I model, the LHC-300 fb<sup>-1</sup>, LHC-3000 fb<sup>-1</sup>, ILC-250 GeV, ILC-500 GeV and ILC-1000 GeV will gradually narrow the allowed range of  $\sin(\beta - \alpha)$ . For the Type-II and Flipped models, the LHC-300 fb<sup>-1</sup> can narrow the ranges of  $\sin(\beta - \alpha)$  sizably, and the ILC-250 GeV can not narrow the ranges of  $\sin(\beta - \alpha)$  more visibly than LHC-3000 fb<sup>-1</sup>.

In Fig. 2 and Fig. 3, we project the surviving samples on the planes of the 125 GeV



Higgs couplings. From Fig. 2, for the Type-I model, we find that the allowed ranges of  $R_{HVV}$  and  $R_{Hf\bar{f}}$  are  $0.86 \sim 1.0$  and  $0.8 \sim 1.17$  for the current constraints,  $0.952 \sim 1.0$  and  $0.911 \sim 1.075$  for the LHC-300  $\text{fb}^{-1}$ ,  $0.97 \sim 1.0$  and  $0.948 \sim 1.048$  for the LHC-3000  $\text{fb}^{-1}$ ,  $0.983 \sim 1.0$  and  $0.957 \sim 1.063$  for the ILC-250 GeV,  $0.991 \sim 1.0$  and  $0.977 \sim 1.026$  for the ILC-500 GeV as well as  $0.994 \sim 1.0$  and  $0.984 \sim 1.017$  for the ILC-1000 GeV.

For the Type-II model, in the wrong-sign  $Hd\bar{d}$  and  $Hl\bar{l}$  couplings region, the current data require  $0.785 < R_{HVV} < 0.975$ ,  $-1.3 < R_{Hd\bar{d}} (R_{Hl\bar{l}}) < -0.775$  and  $0.991 < R_{Hu\bar{u}} < 1.027$ . The LHC-300  $\text{fb}^{-1}$  can exclude the wrong-sign  $Hd\bar{d}$  and  $Hl\bar{l}$  couplings region at the  $2\sigma$  level. In the SM-like region, the current data require  $0.995 < R_{HVV} < 1.0$ ,  $0.83 < R_{Hd\bar{d}} (R_{Hl\bar{l}}) < 1.22$  and  $0.92 < R_{Hu\bar{u}} < 1.07$ . The future LHC and ILC experiments will require  $R_{HVV}$  to be very close to 1. The allowed ranges of  $R_{Hd\bar{d}} (R_{Hl\bar{l}})$  and  $R_{Hu\bar{u}}$  are  $0.946 \sim 1.055$  and  $0.979 \sim 1.025$  for the LHC-300  $\text{fb}^{-1}$ ,  $0.965 \sim 1.034$  and  $0.986 \sim 1.014$  for the LHC-3000  $\text{fb}^{-1}$ ,  $0.965 \sim 1.038$  and  $0.981 \sim 1.015$  for the ILC-250 GeV,  $0.981 \sim 1.019$  and  $0.99 \sim 1.009$  for the ILC-500 GeV as well as  $0.986 \sim 1.014$  and  $0.993 \sim 1.006$  for the ILC-1000 GeV.

For the Lepton-specific model, in the wrong-sign  $Hl\bar{l}$  coupling region, the current data require  $0.915 < R_{HVV} < 0.995$ ,  $-1.3 < R_{Hl\bar{l}} < -0.675$  and  $0.992 < R_{Hu\bar{u}} (R_{Hd\bar{d}}) < 1.01$ . The LHC-300  $\text{fb}^{-1}$ , LHC-3000  $\text{fb}^{-1}$  and ILC-250 GeV can gradually constrain the absolute values of Higgs couplings to  $f\bar{f}$  and  $VV$  to be close to SM values in the wrong-sign  $Hl\bar{l}$  coupling region, and the ILC-1000 GeV can exclude the whole wrong-sign  $Hl\bar{l}$  coupling region at the  $2\sigma$  level. In the SM-like region, the current data require  $0.986 < R_{HVV} < 1.0$ ,  $0.675 < R_{Hl\bar{l}} < 1.288$  and  $0.9 < R_{Hu\bar{u}} (R_{Hd\bar{d}}) < 1.085$ . The future LHC-300  $\text{fb}^{-1}$  will require  $R_{HVV}$  to be in the range of 0.998 and 1.0. The other future LHC and ILC experiments will require  $R_{HVV}$  to be very close to 1. The allowed ranges of  $R_{Hu\bar{u}} (R_{Hd\bar{d}})$  and  $R_{Hl\bar{l}}$  are  $0.97 \sim 1.03$  and  $0.901 \sim 1.091$  for the LHC-300  $\text{fb}^{-1}$ ,  $0.982 \sim 1.018$  and  $0.94 \sim 1.058$  for the LHC-3000  $\text{fb}^{-1}$ ,  $0.988 \sim 1.013$  and  $0.946 \sim 1.051$  for the ILC-250 GeV,  $0.991 \sim 1.01$  and  $0.945 \sim 1.053$  for the ILC-500 GeV as well as  $0.993 \sim 1.007$  and  $0.963 \sim 1.037$  for the ILC-1000 GeV.

For the Flipped model, in the wrong-sign  $Hd\bar{d}$  coupling region, the current data require  $0.865 < R_{HVV} < 0.993$ ,  $-1.35 < R_{Hd\bar{d}} < -0.81$  and  $0.991 < R_{Hu\bar{u}} (R_{Hl\bar{l}}) < 1.015$ . The LHC-300  $\text{fb}^{-1}$  can exclude some samples with  $R_{Hd\bar{d}} < -1$  and  $R_{Hu\bar{u}}$  very close to 1. The LHC-3000  $\text{fb}^{-1}$  can exclude the whole wrong-sign  $Hd\bar{d}$  coupling region at the  $2\sigma$  level. In the SM-like region, the current data require  $0.996 < R_{HVV} < 1.0$ ,  $0.825 < R_{Hd\bar{d}} < 1.195$

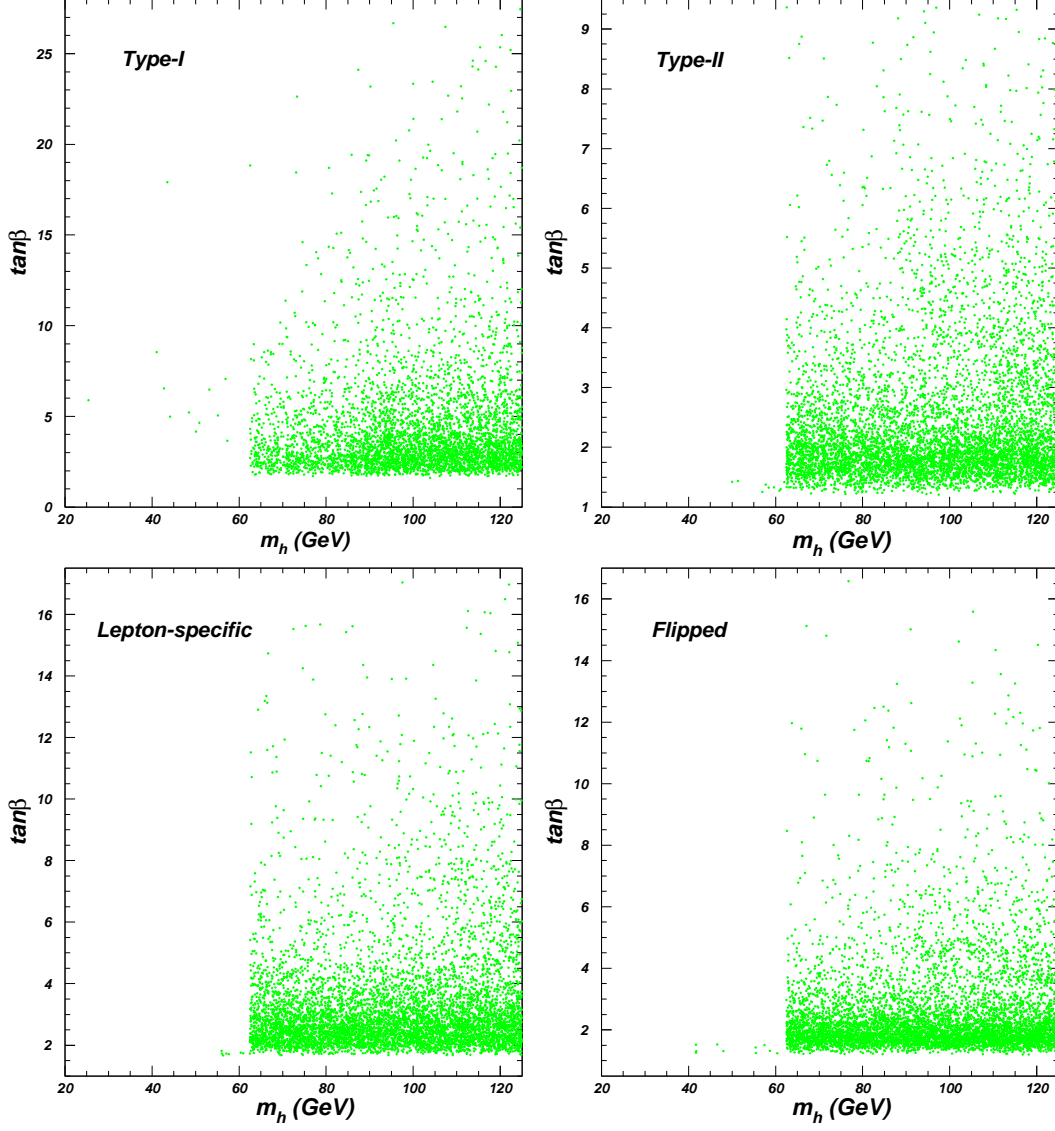


FIG. 4: The scatter plots surviving the current limits projected on the planes of  $m_h$  versus  $\tan \beta$ .

and  $0.932 < R_{Hu\bar{u}} (R_{H\bar{u}l}) < 1.064$ . The future LHC and ILC experiments will require  $R_{HVV}$  to be very close to 1. The allowed ranges of  $R_{Hd\bar{d}}$  and  $R_{Hu\bar{u}} (R_{H\bar{u}l})$  are  $0.946 \sim 1.056$  and  $0.981 \sim 1.018$  for the LHC-300  $\text{fb}^{-1}$ ,  $0.965 \sim 1.034$  and  $0.988 \sim 1.015$  for the LHC-3000  $\text{fb}^{-1}$ ,  $0.97 \sim 1.032$  and  $0.986 \sim 1.013$  for the ILC-250 GeV,  $0.983 \sim 1.018$  and  $0.992 \sim 1.008$  for the ILC-500 GeV as well as  $0.987 \sim 1.013$  and  $0.994 \sim 1.005$  for the ILC-1000 GeV.

Now we examine the allowed mass ranges of the light CP-even Higgs, pseudoscalar and charged Higgs with the heavy CP-even Higgs being the 125 GeV Higgs. Since the focus of this paper is studying the limits on the heavy CP-even Higgs with mass 125 GeV at the current and future collider, the projected limits on  $m_h$ ,  $m_A$  and  $m_{H^\pm}$  from the future collider

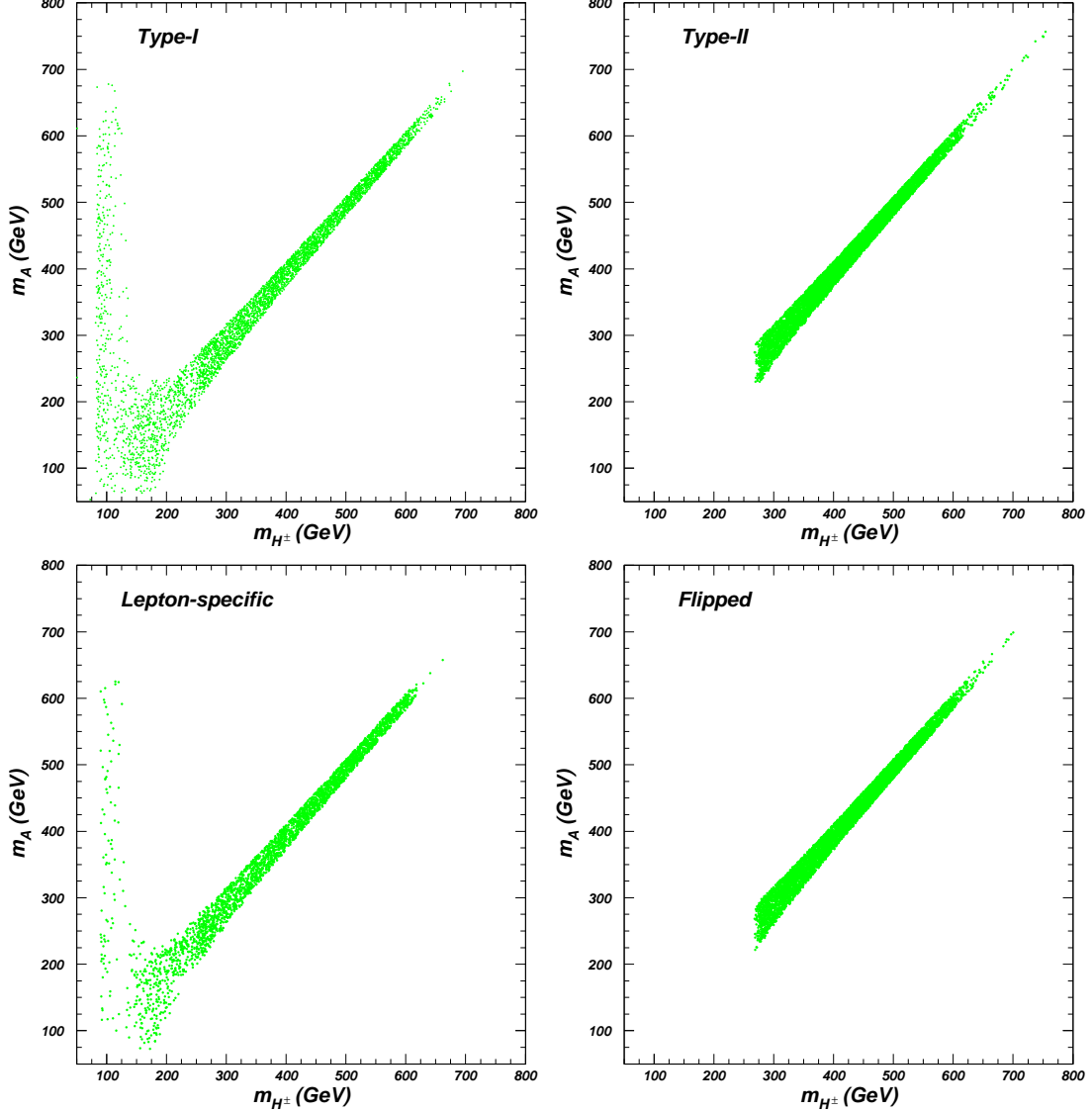


FIG. 5: Same as Fig. 4, but projected on the planes of  $m_{H^\pm}$  versus  $m_A$ .

are beyond the scope of this paper. Therefore, we only show the mass ranges of  $m_h$ ,  $m_A$  and  $m_{H^\pm}$  allowed by the current limits in Fig. 4 and Fig. 5. Since the decay  $H \rightarrow hh$  is open for  $m_h < 62.5$  GeV, the  $BR(H \rightarrow hh)$  has to be small enough that  $H$  can fit the LHC Higgs signal data at an adequate level. As a result, we only obtain a few scattering of points for  $m_h < 62.5$  GeV in the Type-I, Type-II, Lepton-specific, and Flipped models, respectively, as shown in Fig. 4. If a very "fine-tuned" scan is employed, the more low- $m_h$  points may be obtained.

Fig. 5 shows that  $m_{H^\pm}$  is required to be larger than 250 GeV in the Type-II and Flipped models due to the constraints from the low energy flavor observables. There is small mass

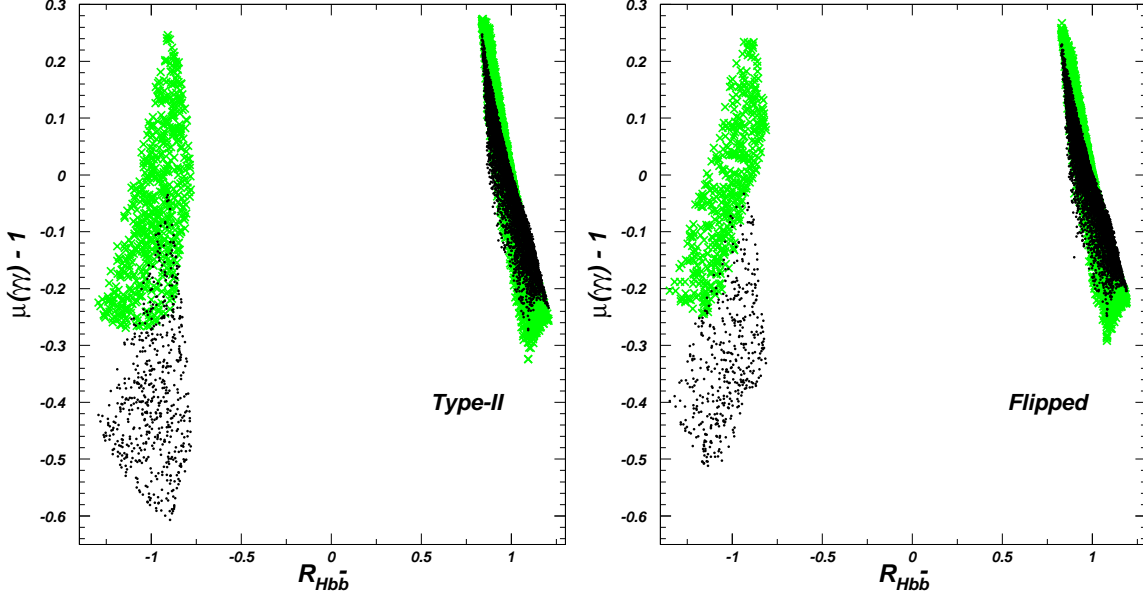


FIG. 6: The scatter plots surviving the current limits projected on the planes of  $R_{Hb\bar{b}}$  versus the diphoton Higgs signal at the LHC and ILC. The crosses (green) denote the inclusive diphoton Higgs signal at the LHC, and the plots (black) denote the diphoton Higgs signal via  $Z$  Higgsstrahlung or  $WW$  fusion at the ILC.

difference between  $m_A$  and  $m_{H^\pm}$  mainly due to the constraints of  $\Delta\rho$ . Since there is small mass difference between  $m_h$  and  $m_H$ ,  $m_A$  and  $m_{H^\pm}$  should have the small mass difference to cancel the contributions of  $m_h$  and  $m_H$  to  $\Delta\rho$ . In the Type-I and Lepton-specific models, since the charged Higgs Yukawa couplings are suppressed by  $\frac{1}{\tan\beta}$ ,  $m_{H^\pm}$  is allowed to be smaller than 100 GeV. Further, for  $m_{H^\pm}$  is around  $m_H$ , the contributions to  $\Delta\rho$  from  $(m_h, m_{H^\pm})$  and  $(m_A, m_{H^\pm})$  loops can be canceled by the  $(m_h, m_H)$  and  $(m_A, m_H)$  loops. Thus  $m_A$  is allowed to have large mass difference from  $m_{H^\pm}$  for  $m_{H^\pm}$  is around 100 GeV.

Ref. [85] shows that the second light Higgs boson explanation of 125 GeV in the MSSM is ruled out by the present experiments. Compared to Type-II model, the five Higgs masses in the MSSM are not independent. Taking the mass of the second light Higgs boson as 125 GeV, the mass of charged Higgs should be smaller than 200 GeV, which is excluded by the current experimental constraints, especially for  $BR(B \rightarrow X_s \gamma)$ . Similarly, the current experimental constraints require  $m_{H^\pm} > 250$  GeV in the Type-II model. However, the Higgs masses in the Type-II model are independent, and we can take enough large  $m_{H^\pm}$  to avoid the current experimental constraints.

For the wrong-sign Yukawa coupling of  $b$ -quark, the interference between the  $b$ -quark and

top-quark loops can give an enhanced contribution to the effective coupling  $hgg$ , and the interference between the  $b$ -quark and  $W$  boson loops can give a suppressed contribution to the effective coupling  $h\gamma\gamma$ . In Fig. 6, we show the inclusive diphoton Higgs signal strength at the LHC and the diphoton Higgs signal strength via  $Z$  Higgsstrahlung and  $WW$  fusion at the ILC (The diphoton Higgs signal strength in the 2HDMs is the same for the  $Z$  Higgsstrahlung and  $WW$  fusion processes at the ILC). The diphoton Higgs rate at the ILC for  $R_{Hb\bar{b}} < 0$  is sizably smaller than those for  $R_{Hb\bar{b}} > 0$ . According to the projected sensitivities of diphoton signal shown in the Table III, the diphoton Higgs rates are within  $2\sigma$  range of ILC-250 GeV  $-1.3 < R_{Hb\bar{b}} < 1.2$ , and ILC-500 GeV for  $R_{Hb\bar{b}} > 0$ , and the ILC-1000 GeV can probe the wrong-sign Yukawa coupling of  $b$ -quark in the Type-II and Flipped models by measuring the diphoton Higgs signal via  $WW$  fusion at  $2\sigma$  level. By measuring the inclusive diphoton Higgs signal at the LHC-300 fb $^{-1}$ , CMS can detect the wrong-sign Yukawa coupling of Type-II model and Flipped model at  $2\sigma$  level.

Assuming the light CP-even Higgs is the discovered 125 GeV Higgs, Ref. [40] shows  $\tan\beta$  and  $\cos(\beta - \alpha)$  within  $2\sigma$  ranges of the current Higgs data and the projected limits from the future collider. Similar to the heavy CP-even Higgs, the wrong-sign Yukawa coupling is absent in the Type-I model, and can appear in the Type-II, Lepton-specific and Flipped models for  $\tan\beta > 3$ . For the Type-II, Lepton-specific and Flipped models,  $\cos(\beta - \alpha)$  is strongly constrained in the SM-like region, and  $\cos(\beta - \alpha)$  in the wrong-sign Yukawa coupling region is allowed to be much larger than that in the SM-like region. The current Higgs data allow  $\cos(\beta - \alpha)$  to be as large as 0.55 for the Type-I, Type-II and Flipped models, and 0.5 for the Lepton-specific model. The ILC-1000 GeV can give the strongest constraints on  $\cos(\beta - \alpha)$ ,  $|\cos(\beta - \alpha)| < 0.4\%$  for the Type-II, Lepton-specific and Flipped models as well as  $|\cos(\beta - \alpha)| < 8\%$  for the Type-I model. For the heavy CP-even Higgs as the 125 GeV Higgs, this paper shows that the ILC-1000 GeV gives the similar constraints on  $\sin(\beta - \alpha)$ ,  $|\sin(\beta - \alpha)| < 10\%$  for the Type-I model,  $|\sin(\beta - \alpha)| < 0.8\%$  for the Type-II model and Flipped models, and  $|\sin(\beta - \alpha)| < 1.4\%$  for the Lepton-specific model. This leads to that  $R_{HVV}$  is very close to 1 due to  $R_{HVV} = \cos(\beta - \alpha) \simeq 1 - \frac{1}{2}\sin(\beta - \alpha)^2$ .

## V. CONCLUSION

In this paper, we assume the 125 GeV Higgs discovered at the LHC is the heavy CP-even Higgs of the Type-I, Type-II, Lepton-specific and Flipped 2HDMs, and examine the parameter space allowed by the latest Higgs signal data, the non-observation of additional Higgs at the collider, and the theoretical constraints from vacuum stability, unitarity and perturbativity as well as the experimental constraints from the electroweak precision data and flavor observables. We obtain the following observations:

(i) The current theoretical and experimental constraints favor a small  $\tan\beta$ , but give a lower limit of  $\tan\beta$ ,  $\tan\beta > 1.6$  for the Type-I model,  $\tan\beta > 1.1$  (2.5) for the SM-like region (wrong-sign Yukawa coupling region) of the Type-II model,  $\tan\beta > 1.6$  (4.0) for the SM-like region (wrong-sign Yukawa coupling region) of the Lepton-specific model, and  $\tan\beta > 1.1$  (3.0) for the SM-like region (wrong-sign Yukawa coupling region) of the Flipped model.

(ii) For the Type-I model, the current experimental data require  $0.86 < R_{HVV} < 1.0$  and  $0.8 < R_{Hf\bar{f}}(u, d, l) < 1.17$ .

(iii) For the Type-II model, the current experimental data require  $0.785 < R_{HVV} < 0.975$ ,  $-1.3 < R_{Hd\bar{d}}(R_{H\bar{l}l}) < -0.775$  and  $0.991 < R_{Hu\bar{u}} < 1.027$  in the wrong-sign  $Hd\bar{d}$  and  $H\bar{l}l$  couplings region, and  $0.995 < R_{HVV} < 1.0$ ,  $0.83 < R_{Hd\bar{d}}(R_{H\bar{l}l}) < 1.22$  and  $0.92 < R_{Hu\bar{u}} < 1.07$  in the SM-like region.

(iv) For the Lepton-specific model, the current experimental data require  $0.915 < R_{HVV} < 0.995$ ,  $-1.3 < R_{H\bar{l}l} < -0.675$  and  $0.992 < R_{Hu\bar{u}}(R_{Hd\bar{d}}) < 1.01$  in the wrong-sign  $H\bar{l}l$  coupling region, and  $0.986 < R_{HVV} < 1.0$ ,  $0.675 < R_{H\bar{l}l} < 1.288$  and  $0.9 < R_{Hu\bar{u}}(R_{Hd\bar{d}}) < 1.085$  in the SM-like region.

(v) For the Flipped model, the current experimental data require  $0.865 < R_{HVV} < 0.993$ ,  $-1.35 < R_{Hd\bar{d}} < -0.81$  and  $0.991 < R_{Hu\bar{u}}(R_{H\bar{l}l}) < 1.015$  in the wrong-sign  $Hd\bar{d}$  coupling region, and  $0.996 < R_{HVV} < 1.0$ ,  $0.825 < R_{Hd\bar{d}} < 1.195$  and  $0.932 < R_{Hu\bar{u}}(R_{H\bar{l}l}) < 1.064$  in the SM-like region.

Further, we give the projected limits on  $\tan\beta$ ,  $\sin(\beta - \alpha)$ ,  $Hf\bar{f}$  and  $HVV$  couplings from the future measurements of the 125 GeV Higgs at the LHC and ILC, including the LHC-300  $\text{fb}^{-1}$ , LHC-3000  $\text{fb}^{-1}$ , ILC-250 GeV, ILC-500 GeV and ILC-1000 GeV. Assuming that the future Higgs signal data have no deviation from the SM expectation, the LHC-300  $\text{fb}^{-1}$ ,

LHC-3000 fb<sup>-1</sup> and ILC-1000 GeV can exclude the wrong-sign Yukawa coupling regions of the Type-II, Flipped and Lepton-specific models at the 2 $\sigma$  level, respectively. The future experiments at the LHC and ILC will constrain the Higgs couplings to be very close to SM values, especially for the  $HVV$  coupling.

### Acknowledgment

This work was supported by the National Natural Science Foundation of China (NNSFC) under grant No. 11105116.

- 
- [1] S. Chatrchyan et al. [CMS Collaboration], Phys. Lett. B **716**, 30 (2012).
  - [2] G. Aad et al. [ATLAS Collaboration], Phys. Lett. B **716**, 1 (2012).
  - [3] Plenary talk by M. Kado, "Phyiscis of the Brout-Englert-Higgs boson in ATLAS", ICHEP 2014, Spain.
  - [4] Plenary talk by A. David , "Phyiscis of the Brout-Englert-Higgs boson in CMS", ICHEP 2014, Spain.
  - [5] G. Aad et al. [ATLAS Collaboration], arXiv:1408.7084.
  - [6] V. Khachatryan et al. [CMS Collaboration], arXiv:1407.0558.
  - [7] G. Aad et al. [ATLAS Collaboration], arXiv:1406.3827.
  - [8] S. Chatrchyan et al. [CMS Collaboration], Phys. Rev. D **89**, 092007 (2014).
  - [9] Talk by C. Mills, "Measurement of Cross Sections and Couplings of the Higgs Boson in the WW decay Channel using the ATLAS detector", ICHEP 2014, Spain.
  - [10] S. Chatrchyan et al. [CMS Collaboration], JHEP **1401**, 096 (2014).
  - [11] S. Chatrchyan et al. [CMS Collaboration], Phys. Rev. D **89**, 012003 (2014).
  - [12] S. Chatrchyan et al. [CMS Collaboration], JHEP **1405**, 104 (2014).
  - [13] Talk by E. Shabalina, "Search for Higgs Bosons produced in association with top quarks with the ATLAS detector", ICHEP 2014, Spain.
  - [14] The CMS Collaboration, "Search for ttH events in the  $H \rightarrow b\bar{b}$  final state using the Matrix Element Method", CMS-PAS-HIG-14-010.
  - [15] Talk by K. Herner, "Studies of the Higgs boson properties at D0", ICHEP 2014, Spain.

- [16] H. E. Haber, G. L. Kane and T. Sterling, Nucl. Phys. B **161**, 493 (1979).
- [17] L. J. Hall and M. B. Wise, Nucl. Phys. B **187**, 397 (1981).
- [18] J. F. Donoghue and L. F. Li, Phys. Rev. D **19**, 945 (1979).
- [19] V. D. Barger, J. L. Hewett and R. J. N. Phillips, Phys. Rev. D **41**, 3421 (1990).
- [20] Y. Grossman, Nucl. Phys. B **426**, 3 (1994).
- [21] A. G. Akeroyd and W. J. Stirling, Nucl. Phys. B **447**, 3 (1995).
- [22] A. G. Akeroyd, Phys. Lett. B **377**, 95 (1996).
- [23] A. G. Akeroyd, J. Phys. G **24**, 1983 (1998).
- [24] M. Aoki, S. Kanemura, K. Tsumura and K. Yagyu, Phys. Rev. D **80**, 015017 (2009).
- [25] A. Pich, P. Tuzon, Phys. Rev. D **80**, 091702 (2009).
- [26] P. M. Ferreira, R. Santos, M. Sher, J. P. Silva, Phys. Rev. D **85**, 035020 (2012).
- [27] C.-Y. Chen and S. Dawson, Phys. Rev. D **87**, 055016 (2013).
- [28] B. Grinstein and P. Uttayarat, JHEP **1306**, 094 (2013) [Erratum-ibid. 1309, 110 (2013)].
- [29] B. Coleppa, F. Kling, S. Su, JHEP **1401**, 161 (2014).
- [30] O. Eberhardt, U. Nierste, M. Wiebusch, JHEP **07**, 118 (2013).
- [31] C. -W. Chiang and K. Yagyu, JHEP **1307**, 160 (2013).
- [32] B. Grinstein and P. Uttayarat, JHEP **1306**, 094 (2013).
- [33] C.-Y. Chen, S. Dawson and M. Sher, Phys. Rev. D **88**, 015018 (2013).
- [34] N. Craig, J. Galloway and S. Thomas, arXiv:1305.2424.
- [35] G. Belanger, B. Dumont, U. Ellwanger, J. F. Gunion and S. Kraml, Phys. Rev. D **88**, 075008 (2013).
- [36] D. Lopez-Val, T. Plehn and M. Rauch, JHEP **1310**, 134 (2013).
- [37] S. Choi, S. Jung and P. Ko, JHEP **1310**, 225 (2013).
- [38] L. Wang, X.-F. Han, Phys. Rev. D **87**, 015015 (2013).
- [39] S. Chang, S. K. Kang, J. -P. Lee, K. Y. Lee, S. C. Park and J. Song, arXiv:1310.3374.
- [40] V. Barger, L. L. Everett, H. E. Logan and G. Shaughnessy, Phys. Rev. D **88**, 115003 (2013).
- [41] C.-Y. Chen, arXiv:1308.3487.
- [42] P. M. Ferreira, R. Santos, J. F. Gunion, H. E. Haber, arXiv:1403.4736.
- [43] L. Wang, X.-F. Han, JHEP **1205**, 088 (2012).
- [44] J. Baglio, O. Eberhardt, U. Nierste, M. Wiebusch, arXiv:1403.1264.
- [45] N. Chen, H.-J. He, JHEP **1204**, 062 (2012).



- [46] X.-F. Wang, C. Du, H.-J. He, Phys. Lett. B **723**, 314 (2013).
- [47] T. Abe, N. Chen, H.-J. He, JHEP **1301**, 082 (2013).
- [48] X.-D. Cheng, Y.-D. Yang, X.-B. Yuan, arXiv:1401.6657.
- [49] W. Altmannshofer, S. Gori and G. D. Kribs, Phys. Rev. D **86**, 115009 (2012).
- [50] Y. Bai, V. Barger, L. L. Everett and G. Shaughnessy, Phys. Rev. D **87**, 115013 (2013).
- [51] K. Cheung, J. S. Lee, P.-Y. Tseng, JHEP **1401**, 085 (2014).
- [52] A. Celis, V. Ilisie, A. Pich, JHEP **1307**, 053 (2013).
- [53] A. Celis, V. Ilisie, A. Pich, JHEP **1312**, 095 (2013).
- [54] W. Altmannshofer, S. Gori, G. D. Kribs, Phys. Rev. D **86**, 115009 (2012).
- [55] L. Wang, X.-F. Han, JHEP **1404**, 128 (2014).
- [56] R. A. Battye, G. D. Brawn, A. Pilaftsis, JHEP **1108**, 020 (2011).
- [57] J. R. Espinosa, C. Grojean, M. Muhlleitner, and M. Trott, JHEP **1205**, 097 (2012).
- [58] G. Belanger, B. Dumont, U. Ellwanger, J. F. Gunion, S. Kraml, JHEP **1302**, 053 (2013).
- [59] P. P. Giardino, K. Kannike, M. Raidal, and A. Strumia, JHEP **1206**, 117 (2012).
- [60] J.-J. Cao, Z.-X. Heng, J. M. Yang, Y.-M. Zhang, J.-Y. Zhu, JHEP **1203**, 086 (2012).
- [61] L. Wang, J. M. Yang, J. Zhu, Phys. Rev. D **88**, 075018 (2013).
- [62] X.-F. Han, L. Wang, J. M. Yang, J. Zhu, Phys. Rev. D **87**, 055004 (2013).
- [63] J. S. Lee and P.Y. Tseng, JHEP **1305**, 134 (2013).
- [64] B. Dumont, S. Fichet and G. Gersdorff, JHEP **1307**, 065 (2013).
- [65] K. Cheung, J. S. Lee, and P.-Y. Tseng, arXiv:1407.8236.
- [66] D. Eriksson, J. Rathsmann, O. Stål, Comput. Phys. Commun. **181**, 189-205 (2010); Comput. Phys. Commun. **181**, 833-834 (2010).
- [67] J. Beringer *et al.* (Particle Data Group), Phys. Rev. D **86**, 010001 (2012).
- [68] F. Mahmoudi, Comput. Phys. Commun. **180**, 1579-1673 (2009).
- [69] Y. Amhis *et al.* [Heavy Flavor Averaging Group], arXiv:1207.1158.
- [70] R. Aaij *et al.* [LHCb Collaboration], Phys. Rev. Lett. **110**, 021801 (2013).
- [71] <http://www.slac.stanford.edu/xorg/hfag/rare/2013/radll/index.html>
- [72] P. Bechtle, O. Brein, S. Heinemeyer, G. Weiglein, K. E. Williams, Comput. Phys. Commun. **181**, 138-167 (2010).
- [73] P. Bechtle, O. Brein, S. Heinemeyer, O. Stål, T. Stefaniak, G. Weiglein, K. E. Williams, Eur. Phys. Jour. C **74**, 2693 (2014).

- [74] Particle Data Group, 2013 partial update for the 2014 edition.
- [75] C. Q. Geng and J. N. Ng, Phys. Rev. D **38**, 2857 (1988) [Erratum-ibid. D 41, 1715 (1990)].
- [76] A. Freitas and Y.-C. Huang, JHEP **1208**, 050 (2012) [Erratum-ibid. 1305, 074 (2013)]  
[Erratum-ibid. 1310, 044 (2013)].
- [77] K. Nakamura et al. [Particle Data Group], J. Phys. G **37**, 075021 (2010).
- [78] H. E. Haber, H. E. Logan, Phys. Rev. D **62**, 015011 (2000).
- [79] G. Degrossi, P. Slavich, Phys. Rev. D **81**, 075001 (2010).
- [80] P. Bechtle, S. Heinemeyer, O. Stål, T. Stefaniak, G. Weiglein, arXiv:1403.1582.
- [81] ATLAS Collaboration, ATL-PHYS-PUB-2013-014.
- [82] CMS Collaboration, arXiv:1307.7135.
- [83] ATLAS Collaboration, arXiv:1307.7292.
- [84] D. M. Asner<sup>1</sup> *et al.*, arXiv:1310.0763.
- [85] G. Barenboim, C. Bosch, M. L. López-Ibáñez, O. Vives, JHEP **1311**, 051 (2013).